Caliphate Journal of Science & Technology (CaJoST)

ISSN: 2705-313X (PRINT); 2705-3121 (ONLINE) Research Article

Open Access Journal available at: https://cajost.com.ng/index.php/files and https://www.ajol.info/index.php/cajost/index

DOI: https://dx.doi.org/10.4314/cajost.v7i2.7

Article Info

Received: 8th February 2025

Revised: 2nd April 2025

Accepted: 4th April 2025

[1]Department of Chemistry, Shehu Shagari College of Education, Sokoto State, Nigeria.

[2]Department of Geography, Shehu Shagari College of Education, Sokoto State, Nigeria.

[3]Biotechnology Research and Development Agency.

***Corresponding author's email:**

lawaligada@gmail.com

Cite this: *CaJoST*, 2025, 2, 241-253

Nanoporous Carbon@Graphene Oxide – Mesoporous Silica Composite as an Absorbent for the Removal of Hg (II) from Aqueous Solution

Lawal Abubakar[1*], Muhammad M. Aliyu[2], Abdullahi A. Tambuwal[1], Asmau U. Sulaiman[1], and Hashim Tukur[3]

Heavy metal, especially mercury (Hg), and agricultural waste pollution is now a serious threat to the environment and human life because of the rapid urbanization and industrialization. In order to handle these toxic pollutant particles or their ions, researchers have attempted to develop several adsorbent materials with change of shape, size, architecture, surface charges, and surface biomolecules. With a view of enhancing the efficiency of adsorbent materials, the present study deals with graphene oxide mesoporous silica incorporated nanoporous carbon (NC) derived from palm kernel shell waste towards Hg (II) adsorption. The composite material were characterized via BET specific surface area (1020 m^2/g), field emission scanning electron microscopy (FESEM), and X-ray diffraction analysis (XRD). The NC@GO-MS composite was most suitable for the adsorption of Hg (II) under the influences of pH, adsorbent dosage, initial concentration and contact time. The maximum adsorption efficiency of Hg (II) (212.8 mg/g) was achieved at a pH 4, while Langmuir model fit the equilibrium sorption data best and was fitted with a pseudo-second order kinetic model. Moreover, thermodynamic studies indicated that, the enthalpy, entropy, and Gibbs free energy values show that the adsorption is compatible with spontaneous, favorable, and endothermic reactions. Therefore, based on the results, the synthesized NC@GO-MS composite can serve as a promising candidate for wastewater treatment considering its efficiency, inexpensive, and environmentally friendly source.

Keywords: Graphene oxide, nanoporous carbon, wastewater, characterizations, Hg (II) adsorption.

1. Introduction

The continuous release of sewage wastewater, automobile emissions, and pollutants from industries such as battery manufacturing and mining is a major contributor to aquatic pollution, which can lead to severe brain and mental health issues (Zhou *et al.,* 2024; Ren *et al.,* 2023). One of the United Nations' Sustainable Development Goals (SDGs) aims to achieve clean water and sanitation by 2030. This goal focuses on improving sanitation and hygiene, treating and reusing wastewater, maintaining water quality, using water efficiently to address scarcity, managing water resources effectively, and protecting and restoring ecosystems related to water (SDG, 2020). Among these challenges, mercury contamination from natural and industrial activities has emerged as a significant environmental threat to humans and ecosystems worldwide (Arrifano *et al* 2023; Saha *et al.,* 2023).

At normal standard, mercury is a highly malleable liquid under temperature and pressure. Its name originated from the Latin word hydragyrum, which means a metal that resembles liquid silver (HSDB, 2004). Mercury (Hg) has an atomic number of 80 and is a silver-white liquid at room temperature with freezing and boiling points of -38.83 °C and 356.73 °C, respectively (Balla, 2022). Mercury is well-known for being a bio-accumulative heavy metal with 2220 tonnes of mercury emission and a persistent atmospheric dangerous pollutant in the world (Pavithra *et al.,* 2022). The permissible limit for mercury was determined to be 0.002 mg/L, and it is one of the ten chemicals about which the WHO is alarmed (WHO, 2016).

Mercury is classified into three main groups: elemental mercury, inorganic mercury, and organic mercury. Mercury exists in several forms: inorganic mercury, among which There have been the metallic mercury and mercury vapor (Hg^0) and mercurous mercury (Hg^+) or mercuric mercury (Hg^{++}) salts; organic mercury, also called organometallic, which results from a covalent bond between mercury and a carbon atom of an organic functional group such as a methyl, ethyl, or phenyl group (Ghosh *et al.,* 2022; Hua *et al.,* 2020).

Mercury is now considered an environmental pollutant of high risk to public health because of its high toxicity and mobility in ecosystems, which can be released into the environment and stayed for a long period of time (Shahid *et al.,* 2020). Human activities have been reported to have exacerbated the atmospheric mercury contamination of water, resulting in the absorption of organisms along the food chain, which primarily occurs through anthropogenic and natural sources (Chakraborty *et al.,* 2022; Buch *et al.,* 2017).

The toxicity of mercury, which includes elemental Hg, particle bound Hg, and gaseous divalent cation Hg^{2+} (the most bioavailable mercury), is primarily determined by its chemical transformation when inorganic mercury combines with carbon to form the most toxic methyl mercury (MeHg) (Alalwan *et al.,* 2020; Carolin *et al.,* 2017). According to the World Health Organization, mercury has contributed to a variety of toxic effects in the immune, digestive, and nervous systems, depending on the form and variation of mercury and the rate of exposure (WHO, 2019).

Various materials and methods have been developed to remove mercury ions, including chemical precipitation, ion exchange, electrochemical treatment, reverse osmosis, and adsorption (Efome et al., 2018). Furthermore, many recent different removal technologies have been used to remove mercury from water or wastewater, which includes, chemical hydrogel (Diacon *et al.,* 2024; Jaques *et al.,* 2024; Ebrahimpour and Kazemi, 2023; Cheng *et al.,* 2022; Lei *et al.,* 2021), membrane separation (Rahimi *et al.,* 2024; Cao *et al.,* 2023; Gosh *et al.,* 2022; Albatrni *et al.,* 2021; Castelletto and Boretti, 2021; Hua *et al.,* 2020), electrodialysis (Kabir *et al.,* 2024; Cerrillo-Gonzalez *et al.,* 2023; Juve *et al.,* 2022; Sun *et al.,* 2020), photocatalysis (Qi *et al.,* 2024; Gaggero *et al.,* 2023; Ji *et al.,* 2021), layered double hydroxide (Tong *et al.,* 2024; Xu *et al.,* 2024; Bi *et al.,* 2022) and adsorption. Among these, adsorption has been widely recognized as one of the simplest and most effective ways to remove heavy metal ions from water (Zheng *et al.,* 2025; Georgin *et al.,* 2024).

Various materials have been used as adsorbents over time. While most adsorbents possess specific characteristics like a large surface area, customizable surface functional groups, easy regeneration, environmental safety, and biodegradability, combining these features in a composite material through controlled design can make the material more durable and effective for mercury adsorption. This research is important as it aims to develop alternative composite materials that are fast, robust, efficient, and selective for removing mercury from contaminated water. Additionally, it seeks to provide a deeper understanding of the adsorption and desorption processes, paving the way for creating more durable adsorbent materials. This study used palm kernel shells to produce nanoporous carbon with H_3PO_4, an eco-friendly, affordable, and widely available material. It also explored whether combining the modified nanoporous carbon with a graphene oxide-mesoporous silica composite could enhance the removal of Hg (II) from water using a batch adsorption method.

2. Materials and Methods

2.1 Materials

Nanoporous carbon from palm kernel shell, 1000 mg/L of the standard of $Hg(NO_3)_2$ (Sigma-Aldrich), Sodium hydroxide (Fluka), Tetraethylorthosilicate (TEOS) (R&M Chemicals), Ammonium nitrate (Merck), Ethanol (Sigma-Aldrich), Hexadecyltrimethylammonium bromide (CTAB) (R&M Chemicals) and Graphene oxide (GO) (R&M Chemicals). All chemicals were used as received without any further purification. For solution preparation, deionized water was used throughout this study.

2.2 Synthesis of nanoporous carbon@graphene oxide mesoporous silica composite

With some modifications, Graphene oxide – mesoporous silica (GO-MS) was prepared using the method described in the literature (Patil *et al.,* 2024 and Kaya *et al.,* 2024). CTAB was used as the agent of pore-foaming. CTAB (1.0 g) and NaOH (40 mg) were treated ultrasonically in a typical experiment until the mixture became transparent. Nanoporous carbon (2 g) prepared from palm kernel shell by impregnating with different ratio/percentage of 100%, 10%, 20%, 30% and 40% (w/v) phosphoric acid/palm kernel shell (H_3PO_4/PKS), mixed, stirred for 24 hr and oven dried at 120^0C for 24 hrs. The impregnated PKS sample (20 g) was thermally activated using an electrical tubular furnace in one step activation method for a predetermined time at

500°C with a 20 mL min^{-1} N_2 gas flow for 1hr, was added shortly for few minutes afterward, and graphene oxide (30 mg) was also added shortly afterward to be treated ultrasonically for 3 hours. TEOS (1.0 mL) was added slowly and subjected to magnetic agitation at 40.0 °C for 2 hours, and the mixture was stirred for 12 hours. The resulting product was then centrifuged and washed with warm ethanol. The obtained NC@GO-MS composite containing CTAB was not calcined to remove the surfactant but was instead washed continuously by heating under reflux at 65.0 °C with a mixture of absolute ethyl alcohol and ammonium nitrate.

2.3 Sample characterization

The surface morphology of the synthesized composite material was investigated using scanning electron microscopy (FESEM) (JEOL, JSM6400) and the attenuated total reflection method in the scanned range of 400 to 4000 cm^{-1}. The nitrogen adsorption–desorption isotherm in an autosorb surface area and porosity analyzer (Quantachrome, Boynton Beach, FL, USA), was used to quantify the composite specific surface area, pore size distribution, and pore volume. The NC@GO-MS were degassed at 290 °C for 6 hours under vacuum before the investigations, and the BET and BJH (Barret-Joyner-Halenda) equations were used to calculate the specific surface area and pore size distribution of the sample material, respectively. A typical X-Ray diffraction procedure includes a light source, the sample, and the detector to record the diffracted X-Rays. Diffraction from a known lattice plane was observed at room temperature by varying the wavelength or Braggs angle θ, with patterns ranging from 20 to 80 degrees theta.

2.4 Batch adsorption set-up

The metal removal efficacy of the prepared adsorbents was evaluated through batch adsorption experiments. In a typical experiment, a known mass of the adsorbent was added to a series of 250 mL Erlenmeyer flasks containing 100 mg/L Hg (II) solution, in which 2 hr were spent shaking the flasks at 160 rpm at room temperature. At a required interval of time, a certain portion was taken and the concentration of Hg (II) ions was determined using mercury analyzer (MA – 3Solo Mercury Analyzer). However, percentage removal (%) and amount of Hg (II) ions adsorbed (q_t) was given in equation 1 and 2 respectively.

$$Removal\ (\%) = \frac{C_0 - C_e}{C_0} \times 100 \quad \text{..... (1)}$$

$$q_t = \frac{(C_0 - C_e)V}{M} \quad \text{..... (2)}$$

Where C_0 and C_e represent the initial and equilibrium concentrations (mg/L), V is the volume of solution used, and M is the weight of adsorbent (g). All adsorption experiments were performed in triplicate to adsorption stability.

2.5 pH optimization

The initial solution Hg (II) pH for adsorption was optimized by adjusting the pH solution with 0.1M NaOH or HCl using a pH meter. The experiment was carried out in a 100 ml solution of Hg^{2+} with a concentration of 10 mg/L and an adsorbent dosage of 0.1g, with all other parameters maintained constant.

2.6 Adsorbent dosage optimization

The adsorbent dosages were varied from 0.1 to 0.5 g while all other parameters remained constant: a 100 mL solution of each metal ion at a concentration of 10 mg/L, a contact time of 2 hours, and a pH of 4.

2.7 Adsorption isotherms

The concentrations of mercury ions in a 100 mL solution were varied to 10, 20, 30, 40, and 50 mg/L. At pH 4 and adsorbent dosage of 0.3 g while other parameters remained constant The Langmuir and Freundlich isotherms are two isotherm models used to describe the adsorption characteristics of adsorbents. Using these two adsorption isotherms, the interaction between the equilibrium concentration and the adsorbate was investigated. The separation coefficient (RL) was used, on the other hand, to determine whether the adsorption process was favorable, unfavorable, linear, or irreversible (Jena *et al.,* 2023; Fu *et al.,* 2023).

2.8 Adsorption kinetics

The contact time for Hg (II) ion solution adsorption varies between 15, 30, 60, 90, and 120 minutes. The experiment, however, was conducted at pH 4 and 25 °C with an initial concentration of Hg (II) ion of 30 mg/L. Adsorption kinetics can be calculated using the pseudo-first-order rate equation and pseudo-second-order kinetic model and its presented in equation 3 and 4.

$$\ln(q_e - q_t) = \ln q_e - kt \quad \text{..... (3)}$$

Where q_e denote adsorption equilibrium of Hg (II) (mg/g), q_t is adsorption of Hg (II) at time *t*, and *k* is the rate constant that can be determined by obtaining the slope by plotting $\ln(q_e - q_t)$ versus *t* (min^{-1}).

$$\frac{t}{q_t} = \frac{1}{k_2 q_e^2} + \frac{t}{q_e} \quad \text{..... (4)}$$

Where, *t* denote Hg (II) ion adsorbed at time *t* (min), q_t and q_e represent the amount of metal ion adsorbed at respective time *t* and equilibrium

(mg/g). Moreover, k_2 denote rate constant of second-order adsorption (g/mg min) (Wu and Ge, 2024; Rind *et al.,* 2023).

2.9 Adsorption thermodynamics

The thermodynamic study was carried out by immersing Erlenmeyer flasks in a water bath at temperatures ranging from 25 to 50^0 C, respectively. The experiment was then carried out at pH 4, and the mixture was shaken for 2 hours with an initial concentration of Hg (II) ion of 30 mg/L. The universal gas constant, R, was used to calculate vital thermodynamic parameters such as enthalpy ΔH, entropy ΔS, and Gibbs free energies ΔG. These finding of the studies were calculated by equation 5 and 6.

$$\Delta G = -RT \ln K_d \quad \text{..... (5)}$$

$$\ln K_d = -\frac{\Delta H}{RT} + \frac{\Delta S}{R} \quad \text{..... (6)}$$

Where K_d denotes adsorption equilibrium constant, R denotes universal gas constant (KJ/mol K), and T denotes temperature (Kelvin). Furthermore, slope and intercept values of ΔH and ΔS were calculated by plotting ln K_d against $1/T$, respectively (Abubakar *et al.,* 2023; Khazaei *et al.,* 2018).

3. Results and Discussion

The textural properties (nitrogen adsorption–desorption isotherms surface area, pore size and pore volume) of NC@GO-MS composite is shown in **Table 1.**

Table 1. Textural properties of NC@GO-MS composite

Sample	BET surface area (m^2/g)	Average pore volume (cm^3/g)	Average pore size (nm)
NC@GO-MS	1020	0.787	3.670

The porosity and surface area in composite materials are caused by irregular voids that might be macropores > 50 nm, mesopores 2-50 nm, or even micropores 2 nm in diameter (Lawal *et al.,* 2024). The surface and porosity (average nitrogen adsorption–desorption isotherms) of NC@GO-MS composite is shown in Figure 1. It was being observed that the BET surface area of NC@GO-MS (1020 m^2/g), average pore volume (0.787 cm^3/g) and average pore size (3.670 nm), but, though its Type IV with H3 hysteresis loop (Figure 1) nitrogen adsorption-desorption isotherm, which is consistent with the capillary condensation in the mesoporous materials (Liou *et al.,* 2021; Majoudi *et al.,* 2019).

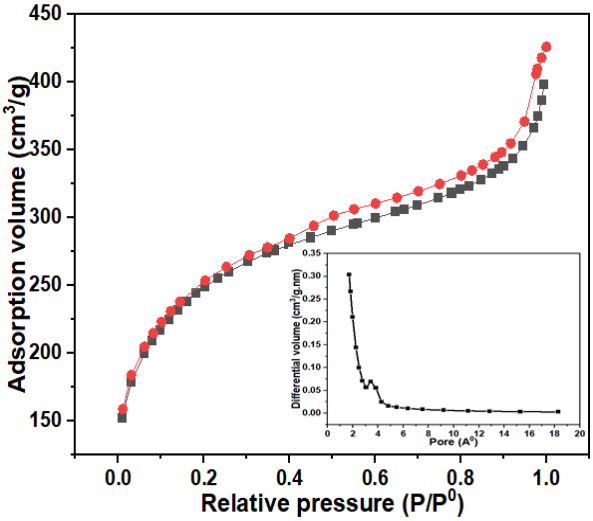

Fig. 1. Isotherms of N_2 adsorption – desorption and pore size distribution of NC@GO-MS

The particle morphology, which is described as micro- or macroporous, is an important characterization related to the adsorption capability of NC@GO-MS. Fig. 2 shows an electron micrograph of the structural morphology of the NC@GO-MS. The composite have a spherical shape, structures, regular and homogeneously covered with precursor which contains well-developed pores where there is the possibility of adsorption of Hg (II) into the surface of the pores and hence enhances the removal of mercury ion from solution (Shen *et al.,* 2021; Majoudi *et al.,* 2019).

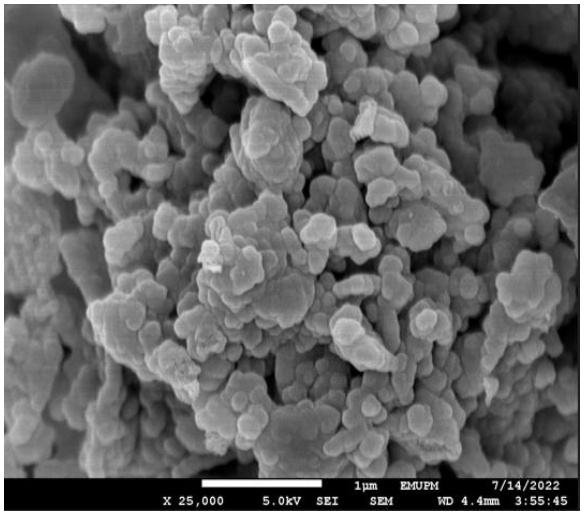

Fig. 2. Fesem morphology of NC@GO-MS

X-ray diffraction was used to examine the phase structure of the carbonized materials (i.e crystalline or armophous) and were shown in Figure 3. After H_3PO_4 treatment, the NC@GO-MS composite exhibited a broad diffraction peak at 2θ = 20–30° corresponding to diffraction (002) attributable to carbon sheets oriented in a random manner, indicating that the graphite has

been fully expanded and successfully oxidized into graphite oxide (Vi *et al.,* 2018), whereas the weak and broad diffraction peak at 40–50˚ corresponding to diffraction (100) is only fairly pronounced for carbonized materials at a temperature of 500˚ C, indicating graphite content, similar to the previous literature reported (Bagbi and Solanki, 2023; Pam *et al.,* 2021).

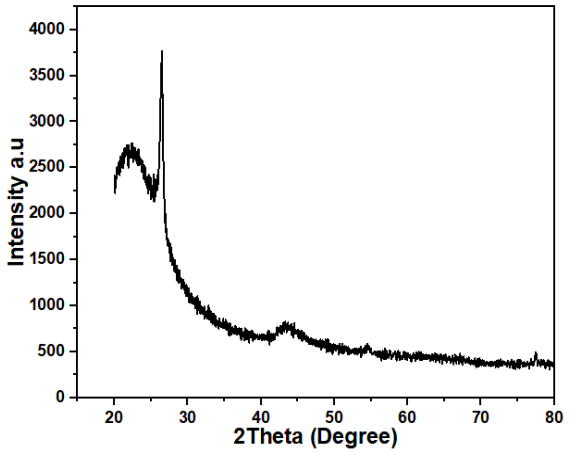

Fig. 3. XRD spectrum of NC@GO-MS composite

3.1 Hg (II) ion adsorption studies of NC@GO-MS composite

The effectiveness of the created adsorbents in removing metal was assessed using batch adsorption experiments. In a standard experiment, we placed a measured amount of a substance that can capture other substances (adsorbent) into a set of 250 mL flasks. These flasks contained a solution with 100 mg/L of Hg (II) ions solution. We then shook these flasks vigorously at room temperature for a duration of 2 hours. At specific time intervals, we collected samples from the flasks, and we measured the concentration of Hg (II) ions in these samples using a specialized instrument called the MA-3Solo Mercury Analyzer. The effects of other variables such as adsorbent dose, contact time, initial ion solution concentration, and reaction temperature on the adsorption of Hg (II) from aqueous solution were then investigated.

3.2 Effect of pH

The pH value has a clear impact on how well carbon-based adsorbents work because it affects the concentration of H^+ ions in water. Since ion exchange and electrostatic interactions depend on H^+ concentration, changes in pH can greatly influence the adsorption process (Duan *et al.,* 2020). The effect of pH on the adsorption of Hg (II) ion onto NC@GO-MS composite were shown in Figure 4. The pH value range was 2 to 6 and with increasing pH value from 2 - 4, the overall adsorption increases from 48.6 mg/g to 95.9 mg/g. At pH 4, the study revealed appreciable adsorption efficiency as a result of availability of negative active site (Mashhadi *et al.,* 2016). Conversely, when the pH value is above 4, the adsorption of Hg (II) ion started to decrease due to interaction between the Hg (II) and proton ion to bind with the OH group leading to the formation of hydroxides of mercury (Liu *et al.,* 2020). In this study, pH 4 was chosen as the optimum pH toward the adsorption of Hg (II) ion and the remaining batch studies.

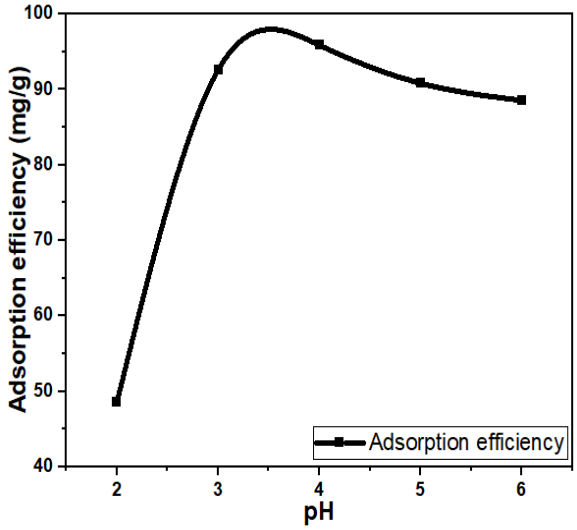

Fig. 4. Effect of pH on Hg (II) ion adsorption efficiency of NC@GO-MS composite

3.3 Effect of absorbent dosage

At an optimal pH of 4, the amount of NC@GO-MS used was varied between 0.1 g and 0.5 g in a 100 mL solution containing 10 mg/L of Hg (II) ions. As shown in Figure 5, the removal efficiency of Hg (II) ions increased as the adsorbent dosage increased, reaching over 89% at 0.1 g and 99% at 0.5 g. This is because a higher dosage provides more adsorption sites and surface area due to the composites structure of the carbon. However, as the adsorbent dosage increased, the amount of Hg (II) ions adsorbed per gram of material decreased from 89 mg/g to 19.8 mg/g. This reduction occurs because the excess active sites lead to lower mixing efficiency and interfere with the mass transfer process, reducing the adsorption capacity per unit mass (Aliprandini *et al.,* 2020). When more than 0.3 g was used, the amount of Hg (II) captured per gram of the adsorbent did not increase significantly. So, 0.3 g of the NC@GO-MS composite was chosen as the optimal amount. It achieved an impressive 97.6% removal rate, with 32.5 mg of Hg (II) adsorbed per gram of the composite.

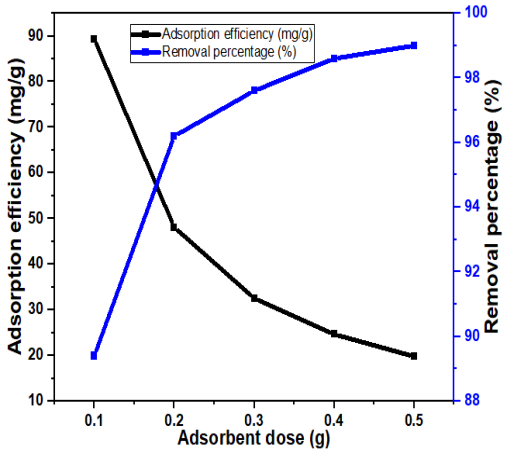

Fig. 5. Effect of adsorbent dose on Hg (II) ion on adsorption efficiency and removal percentage of NC@GO-MS composite

3.4 Effect of Hg (II) ion concentration

The effect of Hg (II) concentration on mercury adsorption was studied by varying the initial concentration from 10 to 50 mg/L in a 100 mL solution. As shown in Figure 6, the experiment was conducted using 0.3 g of adsorbent, with a contact time of 120 minutes, at 25°C, and a pH of 4. The results showed that over 96% of the mercury ions were removed when the initial concentration was low (10 mg/L). This high removal efficiency was due to the lower solute concentration, which meant that the ratio of mercury ions to the available adsorbent surface area was also low (Alqadami *et al.,* 2017). Therefore, the adsorption efficiency of Hg (II) ion increased from 32 to 147.8 mg/g with the increase of initial concentration of Hg (II) ion. This is because as the solution concentration increase, the adsorbent exploited the binding sites to a greater extent, hence increasing the adsorption efficiency (Kenawy *et al.,* 2018; Aliyu *et al.,* 2022b).

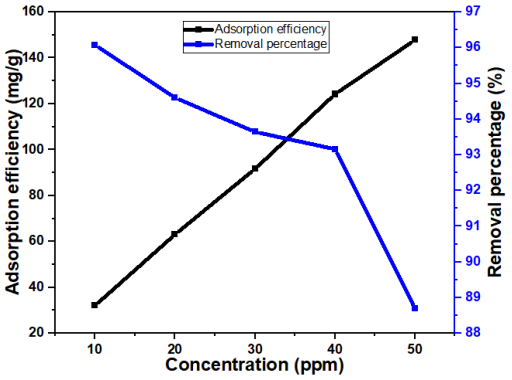

Fig. 6. Effect of initial concentration on Hg (II) ion adsorption efficiency and removal percentage of NC@GO-MS composite

3.5 Effect of contact time

The study was conducted at various contact times; 15, 30, 60, 90 and 120 minutes under the parameters previously optimized. As shown in Figure 7, the Hg (II) ions exhibited a greater adsorption rate on NC@GO-MS composite in the first 15 minutes and raised within 120 minutes; the amount of Hg (II) ions absorbed (q_e, mg/g) was 41.9 and 48 mg/g respectively. The composite surface had a large concentration of free active sites, hence the initial adsorption rate was very high (Goswami *et al.,* 2022; Nyirenda *et al.,* 2022).

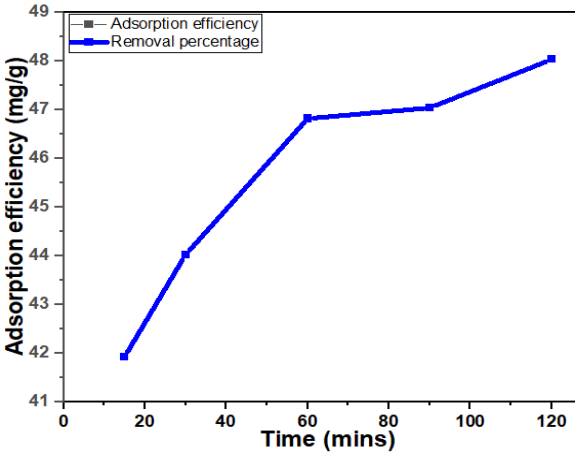

Fig. 7. Effect of contact time on Hg (II) ion adsorption efficiency and removal percentage of NC@GO-MS composite

3.6 Adsorption isotherm studies

To understand how metal ions interact with the adsorbent, an adsorption isotherm was crucial. It helps explain how molecules are distributed between the solid and liquid phases at equilibrium and determines the maximum adsorption capacity. The adsorption capacity of the NC@GO-MS composite for Hg (II) was evaluated by analyzing the data using the Langmuir and Freundlich isotherm models (Aliyu *et al.,* 2022a; Sadegh *et al.,* 2017).

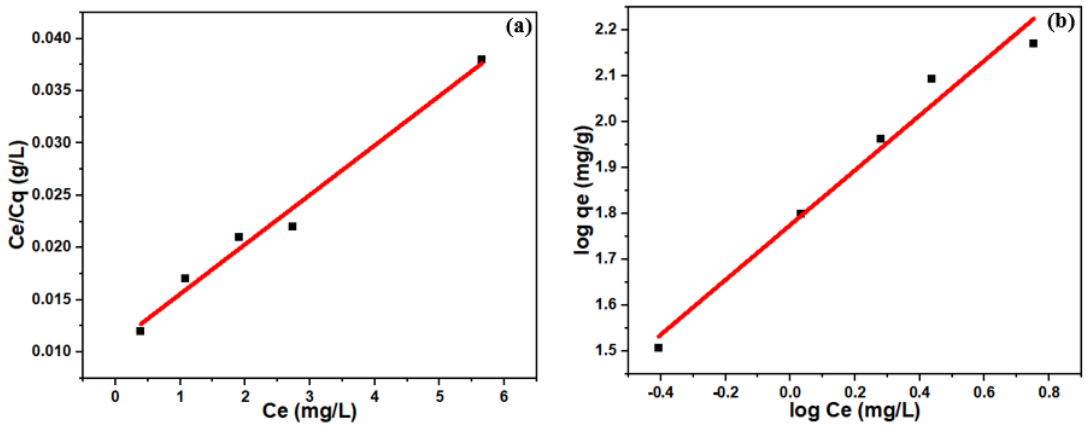

Fig. 8. Langmuir (a) and Freundlich (b) model isotherms for Hg (II) adsorption on NC@GO-MS composite

Table 2. Parameter of the Langmuir and Freundlich isotherm model parameters for Hg (II) adsorption by NC@GO-MS composite

Langmuir isotherm			**Freundlich isotherm**		
Maximum adsorption capacity, (mg/g)	**Langmuir constant, K_L (L/mg)**	**Correlation coefficient, R^2**	**Freundlich constant, K_F (mg/g)**	**Freundlich constant, n**	**Correlation coefficient, R^2**
212.8	0.226	0.9918	4.825	1.673	0.9866

The evaluation was based on the greatest value of the regression plot (R^2) obtained from initial concentration effect data. In this study, R^2 values obtained by linear fitting for the Langmuir and Freundlich models were 0.9918 and 0.9866 for NC@GO-MS composite, as depicted in Figure 8 and Table 2. The adsorption isotherm model of Hg (II) followed the Langmuir model as its correlation coefficient (R^2) value is higher than that of the Freundlich correlation coefficient value. The adsorption mechanism of NC@GO-MS composite to Hg (II) shows that the active adsorbent sites are dispersed equally over the surface and that mercury ions are adsorbed onto the surface (Tran, 2025; Khoo *et al*., 2021).

3.7 Adsorption kinetic studies

The adsorption kinetics of Hg (II) onto the NC@GO-MS composite were analyzed using pseudo-first-order and pseudo-second-order models, as shown in Figure 9. The correlation coefficients (R^2) for these models were 0.8713 and 0.9999, respectively. This indicates that the pseudo-second-order model provided a better fit, suggesting that chemisorption played a key role in the adsorption process (Li *et al.,* 2023; Issa *et al.,* 2022). Additionally, the kinetic parameters for both models are summarized in Table 3.

Table 3. Parameter of the Pseudo-first kinetic and Pseudo-second order model for Hg (II) adsorption by NC@GO-MS composite

Kinetic models	**q_e experimental (mg/g)**	**q_e calculated (mg/g)**	**Correlation coefficient R^2**
Pseudo-first order	48.04	7.464	0.8713
Pseudo-second order	48.04	49.02	0.9999

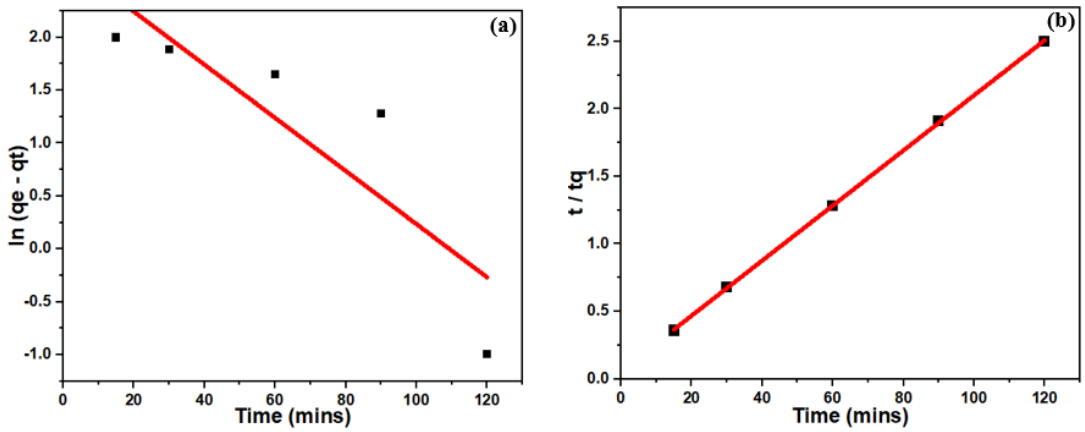

Fig. 9. (a) Pseudo-first order model (b) Pseudo-second order model for Hg (II) adsorption on NC@GO-MS composite

3.8 Adsorption thermodynamic studies

Figure 10a shows how temperature affects the adsorption and removal of Hg (II) by the NC@GO-MS composite. The results indicate that adsorption capacity (mg/g) and removal percentage (%) increased slightly from 63.7 to 64.4 mg/g and 95.6% to 96.6% as the temperature rose from 25°C to 35°C. However, a significant increase was observed, reaching around 65 mg/g and 98%, as the temperature rose further from 40°C to 50°C.

Table 4. Parameter of thermodynamic studies for Hg (II) adsorption NC@GO-MS composite

Temperature K	ΔS (KJ/mol K)	ΔH (KJ/mol)	ΔG (KJ/mol)
298			-4.59
303			-4.80
308	66.47	15.36	-4.99
313			-5.15
323			-6.39

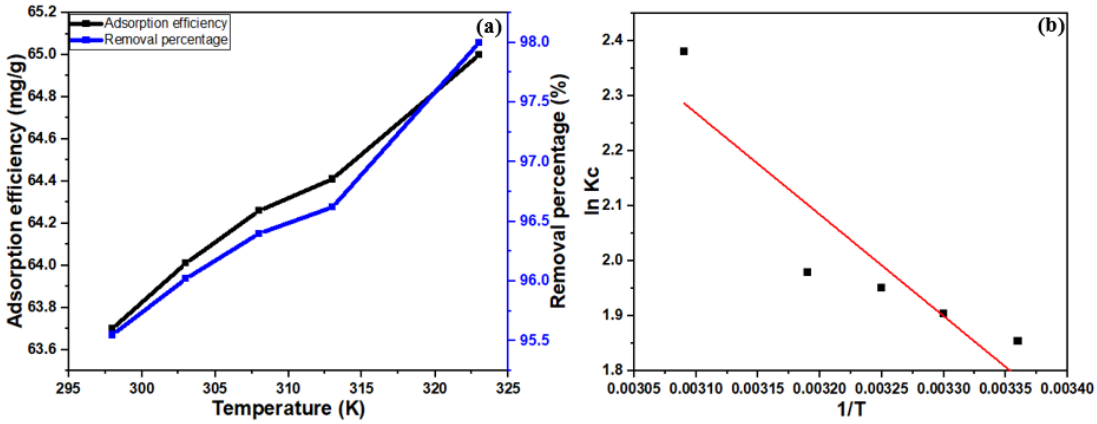

Fig. 10. Effect of temperature for Hg (II) adsorption (a) and Van't Hoff plot used to calculate the activation energy for Hg (II) adsorption (b) on NC@GO-MS composite

Figure 10b highlighted the Van't Hoff plot used to estimate the change of free of energy ΔG, enthalpy ΔH, and entropy ΔS linked with the Hg (II) adsorption mechanism toward NC@GO-MS composite. Moreover, the computed ΔG, ΔH and ΔS are shown in Table 4 above, signifying negative

value of ΔG with increasing temperature, indicating the adsorption mechanism of the absorbent is spontaneous process as a result of constant mobility increment and diffusion of ions into its pores. The positive enthalpy ΔH and entropy ΔS values implied that NC@GO-MS composite adsorption towards Hg (II) is an endothermic reaction and that the probability of favourable adsorption mechanism and randomly increases, displaying a strong affinity between Hg(II) and the absorbate (Abubakar *et al.,* 2023b; Sharma *et al.,* 2023).

4. Conclusion

In conclusion, a nanoporous carbon@graphene oxide mesoporous silica composite for the uptake of Hg (II) from aqueous solution was successfully synthesized. The NC@GO-MS composite was most suitable for the adsorption of Hg (II) under the influences of pH, adsorbent dosage, initial concentration and contact time. In this study, at pH 4, NC@GO-MS composite had a maximum adsorption capacity of 212.8 mg/g towards Hg (II). The adsorption isotherm was well integrated with the Langmuir isotherm model, and the kinetic study was based on the pseudo second-order reaction. Furthermore, the adsorption mechanism fit well with spontaneous and endothermic reactions because it had negative free energy, ΔG°, and positive enthalpy and entropy values. Finally, the synthesized NC@GO-MS composite have shown promise as selective adsorbents of Hg (II) in polluted environments.

Acknowledgements

The authors would like to thank to the Tertiary Education Fund (TETFUND) for supporting this project.

Conflict of Interest

The authors declare no conflict of interest.

References

Abubakar, L., Yusof, N. A., Abdullah, A. H., Wahid, M. H., Abd Rahman, S. F., Mohammad, F., ... & Soleiman, A. A. (2023a). Nanoporous carbon@ CoFe2O4 nanocomposite as a green absorbent for the adsorptive removal of Hg (II) from aqueous solutions. Green Processing and Synthesis, 12(1), 20230169. https://doi.org/10.1515/gps-2023-0169

Abubakar, L., Yusof, N. A., Abdullah, A. H., Mohammad, F., Wahid, M. H., Ismail, S.,. & Soleiman, A. A. (2023b). Molecularly imprinted polymer-based nanoporous carbon nanocomposite for effective adsorption of Hg (II) ions from aqueous suspensions. Separations, 10(8), 454. https://doi.org/10.3390/separations10080454

Alalwan, H. A., Kadhom, M. A., & Alminshid, A. H. (2020). Removal of heavy metals from wastewater using agricultural byproducts. Journal of Water Supply: Research and Technology-Aqua, 69(2), 99-112. https://doi.org/10.2166/aqua.2020.133

Albatrni, H., Qiblawey, H., & El-Naas, M. H. (2021). Comparative study between adsorption and membrane technologies for the removal of mercury. Separation and purification technology, 257, 117833. https://doi.org/10.1016/j.seppur.2020.117833

Aliyu, M., Abdullah, A. H., & bin Mohamed Tahir, M. I. (2022a). Adsorption tetracycline from aqueous solution using a novel polymeric adsorbent derived from the rubber waste. Journal of the Taiwan Institute of Chemical Engineers, 136, 104333. https://doi.org/10.1016/j.jtice.2022.104333

Aliyu, M., Abdullah, A. H., & bin Mohamed Tahir, M. I. (2022b). A Potential Approach for Converting Rubber Waste into a Low-Cost Polymeric Adsorbent for Removing Methylene Blue from Aqueous Solutions. Indonesian Journal of Chemistry, 22(3), 653-665. https://doi.org/ 10.22146/ijc.69674

Aliprandini, P., Veiga, M. M., Marshall, B. G., Scarazzato, T., & Espinosa, D. C. (2020). Investigation of mercury cyanide adsorption from synthetic wastewater aqueous solution on granular activated carbon. Journal of Water Process Engineering, 34, 101154. https://doi.org/10.1016/j.jwpe.2020.101154

Alqadami, A. A., Naushad, M., Abdalla, M. A., Ahamad, T., AlOthman, Z. A., Alshehri, S. M., & Ghfar, A. A. (2017). Efficient removal of toxic metal ions from wastewater using a recyclable nanocomposite: a study of adsorption parameters and interaction mechanism. Journal of Cleaner Production, 156, 426-436. https://doi.org/10.1016/j.jclepro.2017.04.085

Arrifano, G. D. P., Augusto-Oliveira, M., Lopes-Araújo, A., Santos-Sacramento, L., Macchi, B. M., Nascimento, J. L. M. D., & Crespo-Lopez, M. E. (2023). Global Human Threat: The Potential Synergism between Mercury Intoxication and COVID-19. International Journal of Environmental Research and Public Health, 20(5), 4207. https://doi.org/10.3390/ijerph20054207

Baby, R., Hussein, M. Z., Zainal, Z., & Abdullah, A. H. (2023). Preparation of Functionalized Palm Kernel Shell Bio-adsorbent for the treatment of heavy metal-contaminated water. Journal of Hazardous Materials Advances, 10, 100253. https://doi.org/10.1016/j.hazadv.2023.100253

Bagbi, Y., & Solanki, P. R. (2023). Fabrication of Mesoporous Silica Nanoparticle-Decorated Graphene Oxide Sheets for the Effective Removal of Lead (Pb2+) from Water. ACS omega, 9(1), 304-316. https://doi.org/10.1021/acsomega.3c05228

Balla, I. M. E. (2022). Assessment of mercury levels in blood samples among sudanese workers in Abu Hamad Traditional Gold Mining Area in (Doctoral dissertation).

Bi, R., Yin, D., Zhang, S., Zhang, R., & Chen, F. (2022). Efficient removal of Pb (II) and Hg (II) with eco-friendly polyaspartic acid/layered double hydroxide by host-guest interaction. Applied Clay Science, 225, 106536. https://doi.org/10.1016/j.clay.2022.106536

Buch, A. C., Brown, G. G., Correia, M. E. F., Lourençato, L. F., & Silva-Filho, E. V. (2017). Ecotoxicology of mercury in tropical forest soils: Impact on earthworms. Science of the Total Environment, 589, 222-231. https://doi.org/10.1016/j.scitotenv.2017.02.150

Cao, L., Wu, X., He, F., Meng, X., He, W., Li, J., ... & Wang, C. (2023). An Effective Mercury Ion Adsorbent Based on a Mixed-Matrix Polyvinylidene Fluoride Membrane with Excellent Hydrophilicity and High Mechanical Strength. Processes, 12(1), 30. https://doi.org/10.3390/pr12010030

Carolin, C. F., Kumar, P. S., Saravanan, A., Joshiba, G. J., & Naushad, M. (2017). Efficient techniques for the removal of toxic heavy metals from aquatic environment: A review. Journal of environmental chemical engineering, 5(3), 2782-2799. https://doi.org/10.1016/j.jece.2017.05.029

Castelletto, S., & Boretti, A. (2021). Advantages, limitations, and future suggestions in studying graphene-based desalination membranes. RSC advances, 11(14), 7981-8002. https://doi.org/10.1039/D1RA00278C

Cerrillo-Gonzalez, M. D. M., Villen-Guzman, M., Rodriguez-Maroto, J. M., & Paz-Garcia, J. M. (2023). Metal recovery from wastewater using electrodialysis separation. Metals, 14(1), 38. https://doi.org/10.3390/met14010038

Chakraborty, R., Asthana, A., Singh, A. K., Jain, B., & Susan, A. B. H. (2022). Adsorption of heavy metal ions by various low-cost adsorbents: a review. International Journal of Environmental Analytical Chemistry, 102(2), 342-379. doi.org/10.1080/03067319.2020.1722811

Chen, J., Tan, L., Cui, Z., Qu, K., & Wang, J. (2022). Graphene oxide molecularly imprinted polymers as novel adsorbents for solid-phase microextraction for selective determination of norfloxacin in the marine environment. Polymers, 14(9), 1839. /doi.org/10.3390/polym14091839

Cheng, F., Zhang, S., Zhang, L., Sun, J., & Wu, Y. (2022). Hydrothermal synthesis of nanocellulose-based fluorescent hydrogel for mercury ion detection. Colloids and Surfaces A: Physicochemical and Engineering Aspects, 636, 128149. https://doi.org/10.1016/j.colsurfa.2021.128149

Diacon, A., Albota, F., Mocanu, A., Brincoveanu, O., Podaru, A. I., Rotariu, T., ... & Toader, G. (2024). Dual-Responsive Hydrogels for Mercury Ion Detection and Removal from Wastewater. Gels, 10(2), 113. https://doi.org/10.3390/gels10020113

Duan, C., Ma, T., Wang, J., & Zhou, Y. (2020). Removal of heavy metals from aqueous solution using carbon-based adsorbents: A review. Journal of Water Process Engineering, 37, 101339. doi.org/10.1016/j.jwpe.2020.101339

Ebrahimpour, E., & Kazemi, A. (2023). Mercury (II) and lead (II) ions removal using a novel thiol-rich hydrogel adsorbent; PHPAm/Fe3O4@ SiO2-SH polymer nanocomposite. Environmental Science and Pollution Research, 30(5), 13605-13623. https://doi.org/10.1007/s11356-022-23055-z

Efome, J. E., Rana, D., Matsuura, T., & Lan, C. Q. (2018). Metal–organic frameworks supported on nanofibers to remove heavy metals. Journal of Materials Chemistry A, 6(10), 4550-4555. https://doi.org/10.1039/C7TA10428F

Fu, Q., Zhang, T., Sun, X., Zhang, S., Waterhouse, G. I., Sun, C. & Ai, S. (2023). Pyridine-based covalent organic framework for efficient and selective removal of Hg (II) from water: Adsorption behavior and adsorption mechanism investigations. Chemical Engineering Journal, 454, 140154. doi.org/10.1016/j.jece.2022.109228

Gaggero, E., López-Muñoz, M. J., Paganini, M. C., Arencibia, A., Bertinetti, S., Fernández de Paz, N., & Calza, P. (2023). Mercury and organic pollutants removal from aqueous solutions by heterogeneous photocatalysis with ZnO-based materials. Molecules, 28(6), 2650. https://doi.org/10.3390/molecules28062650

Georgin, J., Franco, D. S. P., Dehmani, Y., Nguyen-Tri, P., & El Messaoudi, N. (2024). Current status of advancement in remediation technologies for the toxic metal mercury in the environment: A critical review. Science of The Total Environment, 174501. https://doi.org/10.1016/j.scitotenv.2024.174501

Ghosh, S., Othmani, A., Malloum, A., Christ, O. K., Onyeaka, H., AlKafaas, S. S. & Koduru, J. R. (2022). Removal of mercury from industrial effluents by adsorption and advanced oxidation processes: A comprehensive review. Journal of Molecular Liquids, 120491. https://doi.org/10.1016/j.molliq.2022.120491

Goswami, R., & Dey, A. K. (2022). Synthesis and application of treated activated carbon for cationic dye removal from modelled aqueous solution. Arabian Journal of Chemistry, 15(11), 104290. https://doi.org/10.1016/j.arabjc.2022.104290

HSDB—Hazardous Substances Data Bank, “Mercury,” in Toxicology, Occupational

Medicine and Environmental Series, 2004, http://toxnet.nlm.nih.gov/.

Hua, K., Xu, X., Luo, Z., Fang, D., Bao, R., & Yi, J. (2020). Effective removal of mercury ions in aqueous solutions: A review. Current Nanoscience, 16(3), 363-375. https://doi.org/10.2174/1573413715666190112110659

Issa, M. A., Zentou, H., Jabbar, Z. H., Abidin, Z. Z., Harun, H., Halim, N. A. A. & Pudza, M. Y. (2022). Ecofriendly adsorption and sensitive detection of Hg (II) by biomass-derived nitrogen-doped carbon dots: process modelling using central composite design. Environmental Science and Pollution Research, 29(57), 86859-86872. https://doi.org/10.1007/s11356-022-21844-0

Jaques, L. L., Malheiro, W. C., Jensen, A. T., & Machado, F. (2024). Insights into the synthesis of hydrogels containing glycerol-based macromonomers for wastewater treatment: Focus on the efficient extraction of caffeine and mercury. Journal of Environmental Chemical Engineering, 12(1), 111811. https://doi.org/10.1016/j.jece.2023.111811

Jena, K. K., Reddy, K. S. K., Karanikolos, G. N., & Choi, D. S. (2023). L-Cysteine and silver nitrate based metal sulfide and Zeolite-Y nano adsorbent for efficient removal of mercury (II) ion from wastewater. Applied Surface Science, 611, 155777. doi.org/10.1016/j.apsusc.2022.155777

Ji, S. M., Tiwari, A. P., Oh, H. J., & Kim, H. Y. (2021). ZnO/Ag nanoparticles incorporated multifunctional parallel side by side nanofibers for air filtration with enhanced removing organic contaminants and antibacterial properties. Colloids and Surfaces A: Physicochemical and Engineering Aspects, 621, 126564. https://doi.org/10.1016/j.colsurfa.2021.126564

Juve, J. M. A., Christensen, F. M., Wang, Y., & Wei, Z. (2022). Electrodialysis for metal removal and recovery: A review. Chemical Engineering Journal, 134857. https://doi.org/10.1016/j.cej.2022.134857

Kenawy, I. M., Hafez, M. A. H., Ismail, M. A., & Hashem, M. A. (2018). Adsorption of Cu (II), Cd (II), Hg (II), Pb (II) and Zn (II) from aqueous single metal solutions by guanyl-modified cellulose. International journal of biological macromolecules, 107, 1538-1549. https://doi.org/10.1016/j.ijbiomac.2017.10.017

Kabir, M. M., Sabur, G. M., Akter, M. M., Nam, S. Y., Im, K. S., Tijing, L., & Shon, H. K. (2024). Electrodialysis desalination, resource and energy recovery from water industries for a circular economy. Desalination, 569, 117041. https://doi.org/10.1016/j.desal.2023.117041

Kaya, Ş., Şimşek, V., & Şahin, S. (2024). Investigation of Graphene Oxide/Mesoporous Silica Supports for Enhanced Electrochemical Stability of Enzymatic Electrodes. Catalysis Letters, 154(6), 2701-2712. https://doi.org/10.1007/s10562-023-04520-x

Khazaei, M., Nasseri, S., Ganjali, M. R., Khoobi, M., Nabizadeh, R., Gholibegloo, E., & Nazmara, S. (2018). Selective removal of mercury (II) from water using a 2, 2-dithiodisalicylic acid-functionalized graphene oxide nanocomposite: kinetic, thermodynamic, and reusability studies. Journal of Molecular Liquids, 265, 189-198. https://doi.org/10.1016/j.molliq.2018.05.048

Khoo, Y. T., Tay, K. S., & Low, K. H. (2024). Adsorptive removal of sulphonamides in water by graphene oxide-doped porous polycarbonate derived from optical disc waste. International Journal of Environmental Science and Technology, 21(1), 541-554. https://doi.org/10.1007/s13762-023-05007-3

Lawal, A., Yusof, N. A., Abdullah, A. H., Wahid, M. H., Ismail, S., & Abd Rahman, S. F. (2024). Synthesizing nanoporous carbon from palm kernel shell as a newly designed green absorbent for removing mercury. Chemical Papers, 78(3), 1959-1974. https://doi.org/10.1007/s11696-023-03219-y

Li, Y., Wang, Y., Dou, Z., & Liu, Y. (2023). Removal of gaseous Hg0 using biomass porous carbons modified by an environmental-friendly photochemical technique. Chemical Engineering Journal, 457, 141152. https://doi.org/10.1016/j.cej.2022.141152

Li, H., Li, T., Zhang, T., Zhu, J., Deng, W., & He, D. (2022). Construction and adsorption performance study of GO-CNT/activated carbon composites for high efficient adsorption of pollutants in wastewater. Polymers, 14(22), 4951. https://doi.org/10.3390/polym14224951

Lei, X., Li, H., Luo, Y., Sun, X., Guo, X., Hu, Y., & Wen, R. (2021). Novel fluorescent nanocellulose hydrogel based on gold nanoclusters for the effective adsorption and sensitive detection of mercury ions. Journal of the Taiwan Institute of Chemical Engineers, 123, 79-86. https://doi.org/10.1016/j.jtice.2021.05.044

Liou, T. H., Tseng, Y. K., Liu, S. M., Lin, Y. T., Wang, S. Y., & Liu, R. T. (2021). Green synthesis of mesoporous graphene oxide/silica nanocomposites from rich husk ash: Characterization and adsorption performance. Environmental Technology & Innovation, 22, 101424. https://doi.org/10.1016/j.eti.2021.101424

Liu, Z., Sun, Y., Xu, X., Qu, J., & Qu, B. (2020). Adsorption of Hg (II) in an aqueous solution by activated carbon prepared from rice husk using KOH activation. ACS omega, 5(45), 29231-29242. doi.org/10.1021/acsomega.0c03992

Mashhadi, S., Sohrabi, R., Javadian, H., Ghasemi, M., Tyagi, I., Agarwal, S., & Gupta, V. K. (2016). Rapid removal of Hg (II) from aqueous solution by rice straw activated carbon prepared

by microwave-assisted H2SO4 activation: Kinetic, isotherm and thermodynamic studies. Journal of Molecular Liquids, 215, 144-153. https://doi.org/10.1016/j.molliq.2015.12.040

Mojoudi, F., Hamidian, A. H., Zhang, Y., & Yang, M. (2019). Synthesis and evaluation of activated carbon/nanoclay/thiolated graphene oxide nanocomposite for lead (II) removal from aqueous solution. Water Science and Technology, 79(3), 466-479. https://doi.org/10.2166/wst.2019.071

Nyirenda, J., Kalaba, G., & Munyati, O. (2022). Synthesis and characterization of an activated carbon-supported silver-silica nanocomposite for adsorption of heavy metal ions from water. Results in Engineering, 15, 100553. https://doi.org/10.1016/j.rineng.2022.100553

Pam, A. A., Abdullah, A. H., Tan, Y. P., & Zainal, Z. (2021). Optimizing the route for medium temperature-activated carbon derived from agro-based waste material. Biomass Conversion and Biorefinery, 13(1), 119-130. https://doi.org/10.1007/s13399-021-01597-5

Patil, K. B., Patel, J. K., Goswami, H. H., & Chaudhari, A. S. (2024). Design of Surface Modified Acyclovir-loaded Graphene Oxide-Mesoporous Silica Nanocomposite: Optimization and In Vitro Characterization. Nano Biomedicine & Engineering, 16(3). 10.26599/NBE.2024.9290076

Pavithra, K. G., SundarRajan, P., Kumar, P. S., & Rangasamy, G. (2022). Mercury sources, contaminations, mercury cycle, detection and treatment techniques: A review. Chemosphere, 137314. https://doi.org/10.1016/j.chemosphere.2022.137314

Qi, X., Wang, H., Qian, W., Zhao, S., Gong, C., Yang, X., ... & Yu, E. (2024). Insights into the role of defect engineering for photocatalytic mercury removal from flue gas: A review. Journal of Environmental Chemical Engineering, 112615. https://doi.org/10.1016/j.jece.2024.112615

Rahimi, M., Haghighatjoo, F., & Rahimpour, M. R. (2024). Membrane technologies for mercury removal from natural gas. In Advances Natural Gas: Formation, Processing, and Applications. Volume 5: Natural Gas Impurities and Condensate Removal (pp. 163-181). Elsevier. https://doi.org/10.1016/B978-0-443-19223-4.00001-2

Ren, H., Li, H., Fan, H., Qi, G., & Liu, Y. (2023). Facile synthesis of CoFe2O4-graphene oxide nanocomposite by high-gravity reactor for removal of Pb (II). Separation and Purification Technology, 305, 122472. https://doi.org/10.1016/j.seppur.2022.122472

Rind, I. K., Sarı, A., Tuzen, M., Lanjwani, M. F., & Saleh, T. A. (2023). Synthesis of graphene/silica composites and its removal efficiency of methylene blue dye from water. Inorganic Chemistry Communications, 158, 111507. https://doi.org/10.1016/j.inoche.2023.111507

Sustainable Development Goals, https://www.un.org/sustainabledevelopment/sustainable-development-goals/, (accessed April 2020).

Sadegh, H., Ali, G. A., Gupta, V. K., Makhlouf, A. S. H., Shahryari-Ghoshekandi, R., Nadagouda, M. N., ... & Megiel, E. (2017). The role of nanomaterials as effective adsorbents and their applications in wastewater treatment. Journal of Nanostructure in Chemistry, 7, 1-14. doi.org/10.1007/s40097-017-0219-4

Saha, S., Dhara, K., Chukwuka, A. V., Pal, P., Saha, N. C., & Faggio, C. (2023). Sub-lethal acute effects of environmental concentrations of inorganic mercury on hematological and biochemical parameters in walking catfish, Clarias batrachus. Comparative Biochemistry and Physiology Part C: Toxicology & Pharmacology, 264, 109511. https://doi.org/10.1016/j.cbpc.2022.109511

Shahid, M., Khalid, S., Bibi, I., Bundschuh, J., Niazi, N. K., & Dumat, C. (2020). A critical review of mercury speciation, bioavailability, toxicity and detoxification in soil-plant environment: ecotoxicology and health risk assessment. Science of the total environment, 711, 134749. https://doi.org/10.1016/j.scitotenv.2019.134749

Sharma, S. K., Ranjani, P., Mamane, H., & Kumar, R. (2023). Preparation of graphene oxide-doped silica aerogel using supercritical method for efficient removal of emerging pollutants from wastewater. Scientific Reports, 13(1), 16448. https://doi.org/10.1038/s41598-023-43613-w

Shen, Z., Du, J., Mo, Y., & Chen, A. (2021). Nanocomposites of reduced graphene oxide modified with mesoporous carbon layers anchored by hollow carbon spheres for energy storage. Carbon, 173, 22-30. https://doi.org/10.1016/j.carbon.2020.10.087

Sun, J., Su, X., Liu, Z., Liu, J., Ma, Z., Sun, Y. & Gao, J. (2020). Removal of mercury (Hg (II)) from seaweed extracts by electrodialysis and process optimization using response surface methodology. Journal of Ocean University of China, 19, 135-142. https://doi.org/10.1007/s11802-020-4069-1

Tong, X., Zhang, Z., Dong, X., Guan, W., Liu, Z., Chen, J., ... & Zhang, T. (2024). Sulfur-Intercalated Layered Double Hydroxides Minimize Microbial Mercury Methylation: Implications for In Situ Remediation of Mercury-Contaminated Sites. Environmental Science & Technology, 58(38), 17179-17189. https://doi.org/10.1021/acs.est.4c06870

Tran, H. N. (2025). Some remarks on “Graphene oxide-mesoporous SiO2 hybrid composite for fast and efficient removal of organic cationic contaminants”. Carbon, 233, 119822. https://doi.org/10.1016/j.carbon.2024.119822

Vi, T. T. T., Rajesh Kumar, S., Rout, B., Liu, C. H., Wong, C. B., Chang, C. W., ... & Lue, S. J. (2018). The preparation of graphene oxide-silver nanocomposites: the effect of silver loads on Gram-positive and Gram-negative antibacterial activities. Nanomaterials, 8(3), 163. https://doi.org/10.3390/nano8030163

WHO, Hg and health. World Health Organization. Accessed on September 16, 2019, 2019, https://www.who.int/news.room/fact-sheets/detail/Hg-and-health.

WHO, 2016. The Public Health Impact of Chemicals: Knowns and Unknowns. World Health Organization.

Wu, W., & Ge, H. (2024). Preparation of amino-silane and thiosemicarbazide modified graphene oxide composite for high uptake adsorption of Hg (II) and Pb (II). Journal of Dispersion Science and Technology, 1-12. https://doi.org/10.1080/01932691.2024.2312839

Xu, H., Xu, Y., Zheng, X., Zhang, S., & Guo, Y. (2024). Removal of Hg (II) with MgAl-layered double hydroxide functionalized by schiff base ligands: Application and condition optimization. Chemosphere, 364, 142972. https://doi.org/10.1016/j.chemosphere.2024.142972

Zheng, Y., Li, G., Xing, Y., Xu, W., & Yue, T. (2025). Adsorption removal of mercury from flue gas by metal selenide: A review. Journal of Environmental Sciences, 148, 420-436. https://doi.org/10.1016/j.jes.2023.02.034

Zhou, S., Su, M., Shen, P., Yang, Z., Chai, P., Sun, S., ... & Chen, K. (2024). Association between drinking water quality and mental health and the modifying role of diet: a prospective cohort study. BMC medicine, 22(1), 53. https://doi.org/10.1186/s12916-024-03269-3

